Published online 29 November 2007

Nucleic Acids Research, 2008, Vol. 36, No. 2 ***501–510***
doi:10.1093/nar/gkm1038

Interplay of ion binding and attraction in DNA condensed by multivalent cations

Brian A. Todd* and Donald C. Rau

Laboratory of Physical and Structural Biology, National Institute of Child Health and Human Development, National Institutes of Health, Bethesda, MD 20892-0924, USA

Received July 20, 2007; Revised October 18, 2007; Accepted October 31, 2007

ABSTRACT

We have measured forces generated by multivalent cation-induced DNA condensation using single-molecule magnetic tweezers. In the presence of cobalt hexammine, spermidine, or spermine, stretched DNA exhibits an abrupt configurational change from extended to condensed. This occurs at a well-defined condensation force that is nearly equal to the condensation free energy per unit length. The multivalent cation concentration dependence for this condensation force gives the apparent number of multivalent cations that bind DNA upon condensation. The measurements show that the lower critical concentration for cobalt hexammine as compared to spermidine is due to a difference in ion binding, not a difference in the electrostatic energy of the condensed state as previously thought. We also show that the resolubilization of condensed DNA can be described using a traditional Manning–Oosawa cation adsorption model, provided that cation–anion pairing at high electrolyte concentrations is taken into account. Neither overcharging nor significant alterations in the condensed state are required to describe the resolubilization of condensed DNA. The same model also describes the spermidine^{3+}/Na^{+} phase diagram measured previously.

INTRODUCTION

Interactions between DNA and mobile cations, such as Na^{+}, Mg^{2+} and spermidine^{3+}, play a critical role in DNA physical properties and biological function. Even in dilute solutions of relatively weakly associating monovalent cations, such as Na^{+} and K^{+}, approximately three out of four DNA charges are neutralized by a cation that is in some sense 'bound' (1,2). This neutralization facilitates compaction of DNA into the densely packaged genomes of viruses (3) and cells (4) and deformation of DNA by proteins (5).

Interactions between DNA and monovalent cations seem to be well described by traditional models for polyelectrolyte–counterion interactions, such as Manning–Oosawa theory (6) and the Poisson–Boltzmann equation (7). These theories ignore the interactions among cations and the discrete nature of DNA and counterion charges. In solutions containing only one type of counterion, both theories predict a nearly concentration-independent fraction of DNA charge neutralized. For competitive binding between multiple cations, the binding of each ionic species can be described by a simple adsorption isotherm characterized by an ion- and electrolyte-dependent equilibrium constant (6).

DNA in solutions of tri- and higher-valent cations, such as cobalt hexammine^{3+} and spermine^{4+}, show a peculiar phase behavior not expected for the traditional theories (8–18). DNA initially precipitates at low concentrations of the polyvalent cation and then 'resolubilizes' at high concentration, indicating either decreased neutralization of DNA at elevated concentrations or overcompensation of DNA charge. This deviation from classic adsorption isotherm behavior indicates violations in the basic assumptions in the traditional theories and has been attributed to various causes including correlations between counterions (15,16), increased electrolyte screening (13) and non-ideal polycation–anion pairing at elevated electrolyte concentrations (8,19,20).

Here, we investigate the interactions between polyvalent cations and DNA using single-molecule magnetic tweezers. The measurements extend the existing, mostly structural, data on condensed DNA (21–25) by providing the free energy of condensation across the entire range of condensing conditions. We are able to determine the number of cations associated with DNA by thermodynamic analysis of the electrolyte dependence of condensation free energies. The analysis resolves a subtle increase in the binding of cobalt hexammine^{3+} to DNA as compared to spermidine^{3+} that could not be seen in previous bulk measurements (26,27). The observation of increased binding of $Co(NH_3)_6^{3+}$ to DNA reverses the long-held assumption that $Co(NH_3)_6^{3+}$ condenses DNA at a lower fractional neutralization than spermidine^{3+} (28,29).

*To whom correspondence should be addressed: Tel: +1 301 435 5803; Fax: +1 301 496 2172; Email: toddba@mail.nih.gov

The energetic consequences of these differences in binding are significant and can account for the different phase behavior observed for the two ions. We model the resolubilization of condensed DNA using a traditional Manning–Oosawa cation adsorption model (6). We show that, if ion pairing at high electrolyte concentrations is included, this traditional model can describe resolubilization. Neither overcharging nor electrolyte screening is necessary to describe resolubilization. The same model also describes the spermidine^{3+}/Na^{+} phase diagram previously measured by Raspaud *et al.* (9).

MATERIALS AND METHODS

Magnetic Tweezers

Magnetic tweezing of condensed DNA will be described in more detail in a forthcoming paper (30). Briefly, λ-DNA with multiple biotins at 3′ and 5′ ends was suspended between a fixed 5 μm streptavidin-coated latex bead and a 2.8 μm streptavidin-coated superparamagnetic bead. The stretching force on the DNA was controlled via a micrometer-positioned magnet placed next to a microscope. Condensation forces were measured by stretching the DNA to forces >10 pN, introducing a condensing agent, and then slowly decreasing the force at 0.1 pN/min until it was less than the attractive force of condensation. Condensation was easily observed from the decrease in the stretched length of the DNA from >14 μm to <1 μm. Condensation forces were insensitive to a 2× change in the unloading rate. All measurements were done in solutions containing a background of 10 mM Tris buffer (pH 7.5). We assume throughout an 8 mM monovalent cation concentration, corresponding to ∼80% protonation of Tris.

Measuring the fraction Co^{3+} bound to condensed DNA

High molecular weight DNA prepared from chicken blood was precipitated with spermidine^{3+}/$Co(NH_3)_6^{3+}$ mixtures. The DNA samples (∼200 μg) in screw top Eppendorf tubes were centrifuged at 15 000*g* for 20 min and the buffer removed. The DNA pellets were removed using a glass capillary and transferred to weighing paper. The condensed DNA was gently blotted with lens paper to remove excess buffer. The pellets were transferred back to Eppendorf tubes and dissolved in 1 ml of 1 M NaCl, 10 mM TrisCl (pH 7.5). The absorbance at 475 nm was used to determine the $Co(NH_3)_6^{3+}$ concentration from an extinction coefficient of 0.056/cm mM. Samples were diluted by 100-fold into 10 mM Tris–Cl (pH 7.5), 1 mM EDTA and the absorbance at 260 nm used to determine the DNA concentration from a standard extinction coefficient of 6.7/cm mM DNA-phosphate.

RESULTS

We examined the sensitivity of DNA condensation to multivalent cation concentration by measuring the stretching response of single bacteriophage λ-DNA molecules at different multivalent cation concentrations. In a typical experiment (Figure 1) a molecule is stretched between a large immobilized bead (left-hand side) and a smaller magnetic bead (right-hand side) that exerts a stretching force. Initially stretched by a force >10 pN, the force was gradually decreased (−0.1 pN/min) until the DNA condensed. Prior to condensation, the stretching behavior follows an apparent worm-like chain behavior similar to that previously observed for stretched DNA in the presence of a multivalent cation (dashed line, persistence length 15 nm and contour length of 16.7 μm) (31,32). At a critical condensation force (2.5 pN in this example), the contour length abruptly decreased and the force-extension behavior deviated from the worm-like chain curve (18,31–34). This indicates that ion-mediated attractions between DNA helices were able to overcome the stretching force and the DNA condensed. Over several minutes, the extension progressively decreased until the two beads were nearly touching, indicating complete condensation.

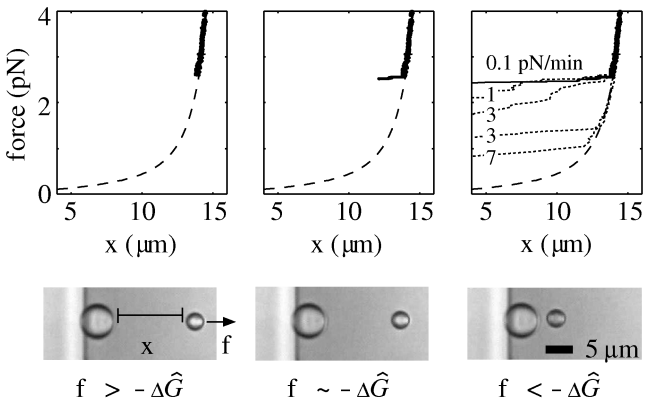

Figure 1. Measuring a condensation force in $Co(NH_3)_6Cl_3$. A single λ-DNA double helix is stretched between an immobilized bead (large bead on the left) and a bead susceptible to a magnetic force pulling to the right. Bathed in a solution containing the multivalent cation, the DNA is initially stretched by a relatively large force, $f > -\Delta\hat{G}$. The force is decreased at 0.1 pN/min and the distance between the beads, x, is monitored. Prior to condensation, the force-distance dependence is well characterized by the worm-like chain model (dashed line). At the condensation force, $f \sim -\Delta\hat{G}$, the bead-bead separation abruptly decreases. Within minutes, condensation of DNA reaches completion, $f < -\Delta\hat{G}$, bringing the magnetic bead nearly into contact with the fixed bead. If the unloading rate was increased to 1–7 pN/min (dashed lines, right-hand plot), the condensation force became stochastic and decreased with increasing unloading rate. This indicates the onset of kinetic effects seen previously (18,32–34).

At this unloading rate of 0.1 pN/min, the condensation forces were insensitive to a 2× increase in unloading rate and condensation of the entire molecule occurred over a narrow, 0.1–0.2 pN, range of force (Figure 1, solid line). This rate independence indicates that, at 0.1 pN/min, the condensation process occurs under quasi-static, equilibrium conditions. Increases in the unloading rate to 1–7 pN/min (Figure 1, dashed lines), progressively decreased the condensation force and introduced a stochastic character. This is similar to the nonequilibrium effects described previously for unloading rates between 1.5 and 5 pN/min (18,32–34). Also similar to previous measurements (18,34), we observed that the reverse process ('decondensation') was rate dependent and required rupture forces of ∼10 pN, even at loading rates of 0.1 pN/min. This indicates that the kinetics of

decondensation are exceptionally slow and that the equilibrium condition for decondensation has not yet been reached at 0.1 pN/min. All of the forces analyzed here are for the equilibrium condensation process measured at an unloading rate of 0.1 pN/min.

The magnitude of the condensation force varied with the concentration and identity of the counterion in solution (Figure 2). As previously observed for spermidine (33), the condensation force for each ion rose from zero at low concentration, reached a peak at some intermediate concentration, and then decreased at higher concentrations. Previously measured critical concentrations for condensation in bulk solution are indicated on Figure 2 by filled arrows (9,24,29). These critical concentrations clearly coincide with zero crossings in our condensation force vs. concentration data. Below the critical concentration, the DNA stretching behavior followed the worm-like-chain curve over the entire range of applied forces (0.01–10 pN; data not shown). For spermidine, we also compare our measurement with a resolubilization concentration measured in the bulk (open arrow) (9). This critical concentration *above* which DNA does not condense also corresponds to a point where the condensation force is zero, this time on the high concentration side of the curve. At all available critical concentrations where, by definition, the total condensation free energy is zero, the condensation force was also zero, consistent with measurement of equilibrium forces.

This result was expected because, at sufficiently slow loading rates, the condensation force is nearly equal to the condensation free energy per unit length (31,32). This can be understood by considering that condensation in the presence of a stretching force is governed by a balance between the favorable (negative) condensation free energy gained by compacting the DNA and the unfavorable (positive) work required to translate the bead against the magnetic force. Spontaneous condensation occurs when the sum of these components is just less than zero, i.e. the applied force is just smaller than the condensation free energy per unit length, $\Delta\hat{G} \sim -f$. At low stretching forces, a bit more accuracy can be achieved by noting that, because the DNA is not completely stretched, the contour length of DNA incorporated into the condensate, L, can be somewhat larger than the distance over which work is done on the bead, ΔX. This gives a slight correction to the free energy, $\Delta\hat{G} = -\Delta x f$, where $\Delta x = \Delta X/L$ can vary between 0 and 1. DNA is >85% stretched for forces >1 pN however, so for most of the forces of interest this contributes a correction of <15%. Nevertheless, we apply this small correction throughout.

Since the equilibrium condensing force is essentially equivalent to the condensation free energy per unit length, our measurements are suitable for thermodynamic analysis. In particular, a Gibbs–Duhem equation links changes in the condensation force to changes in the concentration of multivalent cation salt added to solution, C (Appendix A),

$$\frac{l\Delta x}{k_b T}\frac{\mathrm{d}f_c}{\mathrm{d}\ln C} = \Delta n, \qquad \mathbf{1}$$

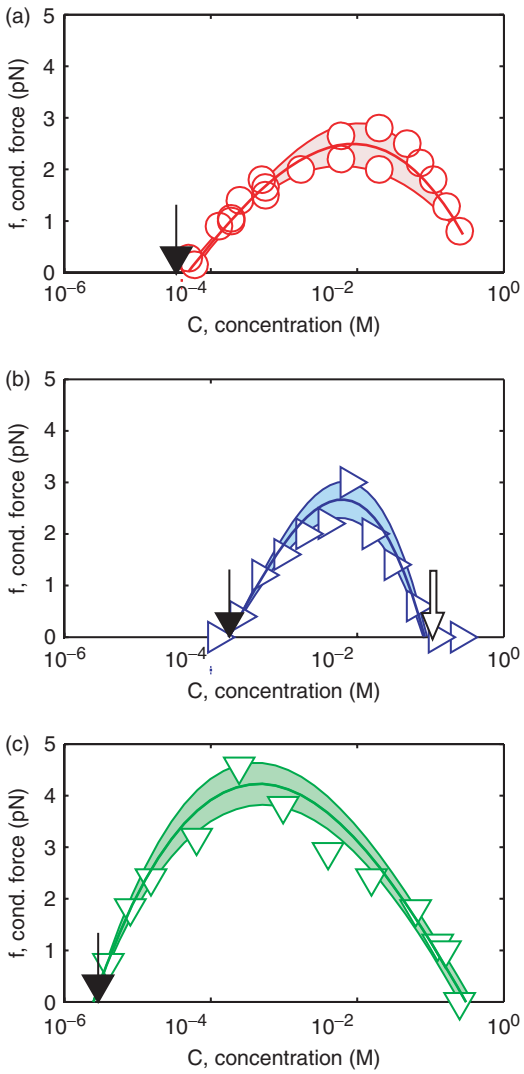

Figure 2. Condensation force as a function of multivalent cation concentration for $Co(NH_3)_6Cl_3$ (**a**), spermidine trichloride (**b**) and spermine tetrachloride (**c**). For each, the condensing force is seen to rise from the critical concentration at low concentration, reaching a peak at intermediate concentration, and then decreasing toward the resolubilization point at high concentration. Where data is available, we have compared our measurement with previous bulk measurements of the critical (filled arrows) and resolubilization concentrations (open arrows). $Co(NH_3)_6Cl_3$ data taken from Matulis *et al.*, spermidine data from Raspaud *et al.* and spermine data extrapolated from Raspaud *et al.* (9,24,29). The zero crossings in our measurements clearly correspond to the borders of the phase diagram measured in the bulk.

where $l = 1.7$ Å is the average contour length between DNA phosphates, k_b is the Boltzmann constant, and T is temperature. In the dilute limit, Δn is the difference in number of +3 ions bound to the condensed and extended DNA per DNA phosphate. At higher concentrations, however, ion activities can be nonideal due to, for instance, ion pairing. In this case, Δn is an 'apparent' difference in bound ions; it represents a weighted contribution from all ion species formed from the incremental addition of multivalent cation 'salt'.

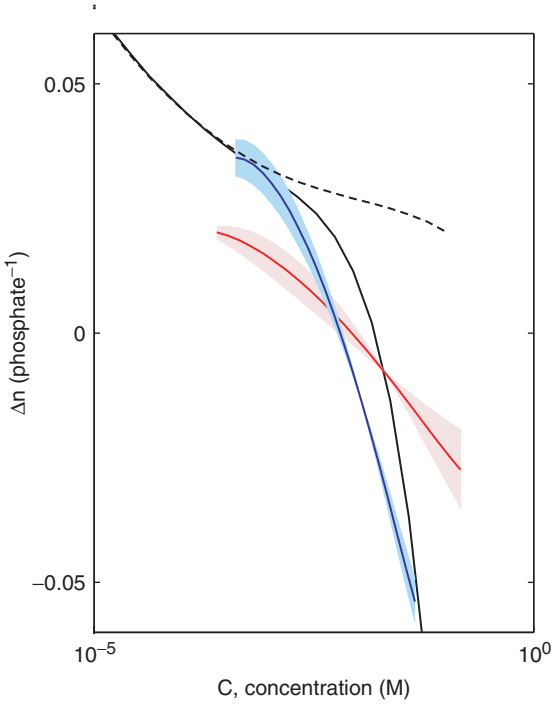

Figure 3. The sensitivity of the condensation free energy to multivalent cation concentration for $Co(NH_3)_6Cl_3$ (red) and spermidine trichloride (blue). At low concentrations, where dissociation of the trivalent cation is complete this equals the change in number of bound trivalent cations accompanying condensation. At their respective critical points, $Co(NH_3)_6^{3+}$ requires binding of 0.01 fewer ion/phosphate than spermidine. Around the critical point, the spermidine curve (blue) is well modeled by Manning–Oosawa counterion association for the competition between the +3 ion and the monovalent Tris buffer (dashed line). At higher concentrations, the experimentally measured sensitivities decrease and become negative. This can be understood as the competition between the +3 form of each multivalent cation and its +2, chloride associated form. The solid line is calculated using a previously estimated equilibrium constant of 0.15 M for the spermidine to spermidine–chloride association and Manning–Oosawa theory. This models contains no free parameters.

This distinction becomes important at high concentrations used in DNA resolubilization experiments. We directly evaluate Δn from the slopes of each curve in Figure 2. The resulting plot (Figure 3) gives the apparent change in number of bound multivalent cations as a function of its concentration.

We will postpone analysis of the higher concentrations until the Discussion section. For now, we restrict ourselves to the trivalent cations, $Co(NH_3)_6^{3+}$ and spermidine^{3+}, and to the dilute regime near the low concentration critical points. In this case, ions are fully dissociated and the apparent change in bound cations is equal to the change in trivalent cations, $\Delta n = \Delta n_{3+}$ (Appendix A). The number of additional ions that must bind for $Co(NH_3)_6^{3+}$ to condense DNA (red) is less than for spermidine (blue) (see that red is lower than blue at low concentrations in Figure 3). This occurs despite the lower critical concentration for $Co(NH_3)_6^{3+}$. The critical concentrations, C_{crit}, and change in number of bound ions at the critical point, Δn_{crit}, are 4.1×10^{-5} M and 0.028 per phosphate for $Co(NH_3)_6^{3+}$ and 1.8×10^{-4} M and 0.038 per phosphate for spermidine.

From Δn_{crit}, C_{crit}, and an estimate of the local concentration of trivalent cations bound to DNA, $C_b = 0.2$ M (1), we can estimate the free energy cost to bind the additional multivalent cations at the critical point,

$$\Delta G_{ion} \sim k_b T \Delta n_{crit} \ln\left[\frac{C_b}{C_{crit}}\right]. \quad \mathbf{2}$$

The free energy costs for $Co(NH_3)_6^{3+}$ and spermidine are identical within the ~10% precision for the measured Δn_{crit} and are equal to $\sim 0.25\, k_b T$/phosphate. This indicates that the ~0.01 ion bound per phosphate decrease in Δn_{crit} for $Co(NH_3)_6^{3+}$ compensates for the increased energetic cost per ion at the more dilute critical concentration. This subtle but measurable difference in ion binding accounts for the lower critical concentration of $Co(NH_3)_6^{3+}$ as compared to spermidine. For both $Co(NH_3)_6^{3+}$ and spermidine, this unfavorable energy required to binding +3 ions is balanced by identical free energies of DNA-DNA interactions and $Tris^{1+}$ release (30).

We sought to quantify the differences in ion binding in terms of binding constants. Because Δn_{3+} represents a difference between cations bound to the condensed and extended DNA, it is unclear in which phase binding differs between $Co(NH_3)_6^{3+}$ and spermidine^{3+}. We assume that the condensed phase is neutralized by both spermidine and $Co(NH_3)_6^{3+}$ and that the difference lies with the fraction bound to the extended phase, $\theta_{3+} = (1/3) - \Delta n_{3+}$. This choice is consistent with the insensitivity of osmotic stress curves of counterion condensed DNA to condensing ion concentration (25,30), with small surface potentials measured in electrophoresis of condensed DNA (10,18), and with spectroscopic measurements that we will present below. We extract binding constants from Scatchard plots of the concentration dependence of θ_{3+} in a manner identical to previous measurements (26,27) and estimated the binding constant uncertainties defined by a 90% confidence interval. The binding constant for $Co(NH_3)_6^{3+}$ ($K_{Co(NH_3)_6^{3+}} = 2.0 \pm 0.6\, \mu M^{-1}$) is 3-fold larger than that for spermidine ($K_{spermidine} = 0.6 \pm 0.3\, \mu M^{-1}$).

We corroborated the relative difference in binding constants between spermidine and $Co(NH_3)_6^{3+}$ using a direct competition binding assay in condensed DNA. The ratio of $Co(NH_3)_6^{3+}$ and DNA in the condensed phase was measured spectrophotometrically after dissolving ~200 μg of condensed DNA in a high salt solution. At 2 mM $Co(NH_3)_6^{3+}$ and in the absence of competing 3^+ spermidine, a $Co(NH_3)_6^{3+}$/DNA-phosphate ratio of 0.33 ±0.01 is measured, consistent with complete neutralization of DNA by $Co(NH_3)_6^{3+}$. In the competition experiment, the sum of cobalt hexammine and spermidine concentrations is held fixed at 2 mM. We assume that electroneutrality is maintained and that the fraction of spermidine bound to DNA is given by the decrease in bound $Co(NH_3)_6^{3+}$, $\theta_{spermidine} = (1/3) - \theta_{Co(NH_3)_6^{3+}}$. For conventionally defined binding constants,

$$K_i = \frac{C_{i-DNA}}{C_i C_{DNA}} = \frac{\theta_i}{C_i}, \quad \mathbf{3}$$

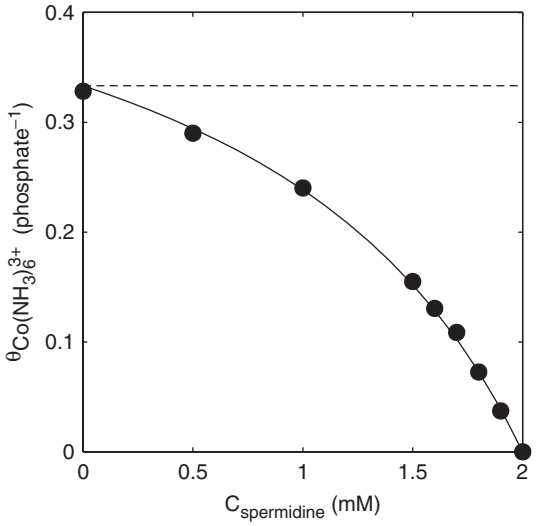

Figure 4. Competitive DNA binding between $Co(NH_3)_6^{3+}$ and spermidine. The $Co(NH_3)_6^{3+}$ concentration relative to the DNA phosphate concentration, $\theta_{Co(NH_3)_6^{3+}}$, is measured as a function of the spermidine concentration, $C_{spermidine}$. A fit of Equation (4) to the data gives relative binding constants, $K_{Co(NH_3)_6^{3+}}/K_{spermidine^{3+}} = 2.5$ (line).

this predicts

$$\theta_{Co(NH^3)_6^{3+}} = \frac{1}{3\left(\frac{C_{spermidine}}{(0.002-C_{spermidine})} \times \frac{K_{Co(NH_3)_6^{3+}}}{K_{spermidine^{3+}}} + 1\right)} \quad 4$$

A fit of Equation (4) with the ratio of binding constants, $K_{Co(NH_3)_6^{3+}}/K_{spermidine^{3+}}$, as the single free parameter gives the solid line in Figure 4. The best fit $K_{Co(NH_3)_6^{3+}}/K_{spermidine^{3+}} = 2.5$ concurs with the binding constants estimated from the concentration dependence of Δn_{3+}. Hence, binding of each cation to condensed DNA is similar to its binding to extended DNA (in the magnetic tweezers measurements), with $Co(NH_3)_6^{3+}$ showing ~3-fold stronger binding than spermidine. Condensation was not expected to affect cation binding because attractive free energies between the two ions differ by <0.05 kT/bp and because the work required to move between the equilibrium interhelical spacings for the two cations is only ~0.05 kT/bp. The predictions of cation binding based on simple equilibrium constants appears to hold equally well in condensed and extended DNA states.

DISCUSSION

Our results highlight the remarkably large effect that small alterations in ion-binding constants can have on DNA condensation. The 0.01 ion/phosphate decrease in $Co(NH_3)_6^{3+}$ required to condense DNA fully accounts for the ~4-fold decrease in critical concentration, as compared to spermidine; decreasing the number of neutralizing ions required to condense DNA allows $Co(NH_3)_6^{3+}$ to condense at a higher cost of mixing entropy per ion. It was previously thought that the more

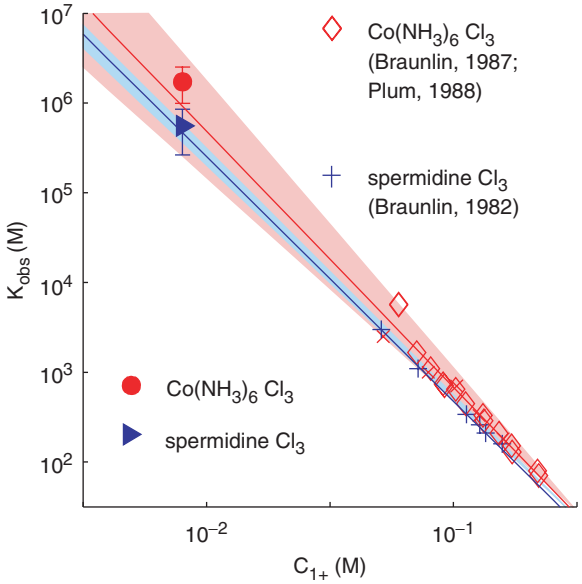

Figure 5. Comparing our measured DNA association constants for $Co(NH_3)_6^{3+}$ (red circle) and spermidine (blue triangle) with previous equilibrium dialysis measurements (red triangles for $Co(NH_3)_6^{3+}$ and blue '+' for spermidine). The current measurements are consistent with extrapolations from the previous measurements (red and blue lines) within experimental error (shaded regions).

compact charge of $Co(NH_3)_6^{3+}$ facilitated stronger, more correlated DNA–DNA electrostatic interactions (16,29,35). However, recent measurements by magnetic tweezers showed that the free energy of direct DNA–DNA interactions for $Co(NH_3)_6^{3+}$ and spermidine condensed DNA are equal (30). Our measurements explain how $Co(NH_3)_6^{3+}$ can condense DNA at a lower critical concentration while facilitating the same direct DNA–DNA interactions.

This conclusion, that differences in ion binding account for differences in spermidine and $Co(NH_3)_6^{3+}$ critical concentrations, is superficially at odds with classic measurements of cation–DNA associations that showed binding of spermidine^{3+} and $Co(NH_3)_6^{3+}$ to be indistinguishable. A plot of our measured binding constants alongside the previous measurements, however, shows that our measurements are consistent with the previous measurements within their experimental uncertainty (Figure 5). The appropriate interpretation of the previous measurements is, therefore, that binding of spermidine^{3+} and $Co(NH_3)_6^{3+}$ to DNA are similar but, within the measurement uncertainty, the difference in condensation critical concentrations 'could be' due to ion binding. Our measurements show that the difference 'is' due to ion binding.

The physical mechanisms responsible for this difference in ion binding are unknown. However, the difference in ion binding that we measure is similar to NMR measurements of a concentration insensitive, 0.02 ion/phosphate population of $^{59}Co(NH_3)_6^{3+}$ tightly bound to extended DNA (36,37). This excess is of the right sign and magnitude to account for the difference in our measurements. This fraction was previously correlated

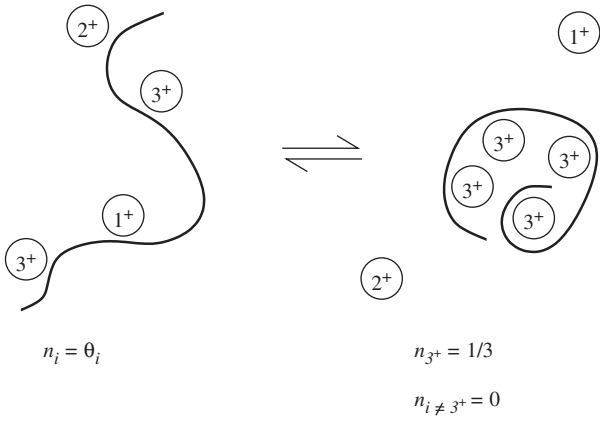

Figure 6. Modeling the electrolyte concentration dependence of the condensation free energy. We assume that the variations in free energy are due solely to the changes in free energy associated with binding counterions upon condensation, neglecting any changes to the condensed state itself. The number of counterions bound to the extended DNA (left side), θ_i, are calculated using Manning–Oosawa counterion association theory. The condensed DNA (right side) is assumed to be completely and exclusively neutralized by the trivalent cation.

to the fraction of stacked guanine–guanine pairs in DNA and thought to be related to a hydrogen bonded bridge that $Co(NH_3)_6^{3+}$ forms between neighboring guanines (36,37). Additionally, at high fractions of bound +3 ions, it should be easier to bind compact $Co(NH_3)_6^{3+}$ that sterically occludes perhaps one base pair compared with extended spermidine^{3+} that could span ~3 base pairs. Whatever the precise mechanism, the consistent interpretation of our results at high cation-binding densities and the equilibrium dialysis measurements at low binding densities highlights the effectiveness of simple binding constants for characterizing DNA–cation interactions over a large range of electrolyte conditions.

Given the strong influence of ion binding on the phase behavior of condensed DNA, we sought to determine how effectively a model describing the changes in free energy associated with ion binding could describe our measured variations in condensation force with electrolyte concentrations. The model, depicted in Figure 6, consists of two simple components. First, the numbers of ions bound to the uncondensed, extended DNA are calculated using Manning–Oosawa counterion association theory (6). This theory makes a number of questionable simplifications, yet experimental measurements of cation binding to DNA tend to confirm its predictions (1). In particular, Manning–Oosawa theory predicts, to within 0.015 cations/DNA phosphate, the change in bound spermidine or cobalt hexammine with incremental changes in the concentration of a lower valent species (26,27,38). Since this is the competition we consider here, Manning–Oosawa theory is expected to be adequate. The second assumption in our model is that the condensed DNA is neutralized completely and exclusively by the 3^+-valent cation. Besteman *et al.* have shown that this is not strictly the case and that DNA condensates move in response to an electric field. However, standard electrokinetic analysis of their measured mobilities via the Smoluchowski and Graham equations, assuming a conservative volume-to-surface ratio for the condensate of 10 nm, gives a fractional charge imbalance of ±0.008 from their measured mobilities. This places rather tight limits on the bound fraction of trivalent cations of 0.331–0.336 cations per phosphate, very similar to our spectrophotometric measurement of 0.33 ± 0.01 $Co(NH_3)_6^{3+}$ per phosphate in the DNA condensates (see Figure 4 at $C_{\text{spermidine}} = 0$). Note that this model says nothing about the DNA–DNA attractive interactions that drive DNA condensation and therefore, we implicitly assume that they do not vary with electrolyte conditions. This is consistent with the insensitivity of the condensed structure, measured by X-ray diffraction, to the concentration of multivalent cations (24,25). Here we focus only on the energetics associated with ion binding and how this varies with electrolyte concentrations.

We first naively assume that the $Co(NH_3)_6Cl_3$ and spermidine trichloride salt fully dissociate, so that, the apparent change in number of ions bound, Δn is equal to the change in number of trivalent ions bound Δn_{3+} (Appendix A). Plotted as the dashed line in Figure 3, Δn_{3+} overlaps the spermidine data at low concentrations where dissociation of the salt is expected to be complete. At higher concentrations, the model plateaus out, indicating saturation of the +3 ion at $\theta_{3+} \sim 0.30$. Deviations of DNA condensation data from this classic adsorption isotherm behavior have attracted considerable attention and have been referred to as 'resolubilization' or 'reentrant transition'. This behavior whereby DNA first precipitates at low concentration of multivalent cations and later 'resolubilizes' at higher concentrations (8–12,18) is also seen in other polyelectrolyte systems (10,13,39) and is thought to represent a fundamental new physics not captured by the conventional saturating adsorption isotherm (6). This has motivated development of new theories for polyelectrolyte–ion interactions (13–17).

Alternatively, Solis and Olvera de la Cruz (19,20) and, independently, Yang and Rau (8) have noted that resolubilization occurs at concentrations where a significant fraction of 3^+ ions associate with anions to form a 2^+-valent anion-paired form. From this point-of-view, the DNA condensate falls apart due to increased competition between the 2^+ and 3^+ forms at high concentrations. The Cl^- dissociation constant has been measured for $Co(NH_3)_6^{+3}$ as 0.02 M (40,41) and has been estimated for spermidine^{+3} as 0.15 M (8), indicating significant quantities of 2^+-valent forms at concentrations approximately >0.01 M. That this sort of ion-pairing occurs should not be surprising given that $Co(NH_3)_6Cl_3$ is insoluble beyond ~0.4 M. Typical resolubilization experiments, similar to the current measurements, approach the solubility limit of the multivalent cation where ion behavior is highly nonideal.

Ion pairing can be incorporated into our model in a straightforward way. Using the estimated dissociation constant for spermidine–Cl^{+2}, for instance, we simply calculate the relative populations of fully dissociated 3^+-valent and partially dissociated 2^+-valent ions. Based on these concentrations, Manning–Oosawa theory is used to calculate the fraction of 3^+ and 2^+ ions bound to the

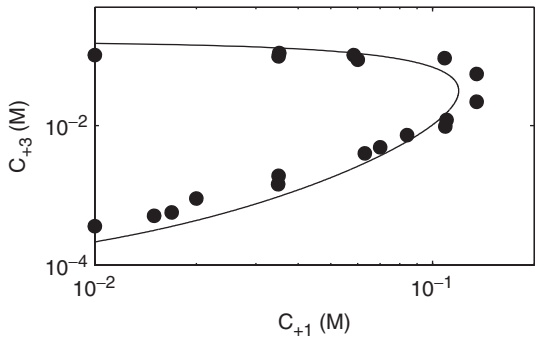

Figure 7. Modeling the spermidine^{3+}/Na^{+} phase diagram, as measured by Raspaud *et al.* (circles). The same model used to describe the multivalent cation concentration dependence of the condensation free energy in Figure 3 also describes the trivalent/monovalent cation phase boundaries (line). This model contains no free parameters.

extended DNA. The apparent change in the number of bound ions now includes contributions from each of these two populations. For this case, the Gibbs–Duhem equation gives (Appendix B),

$$\Delta n = \Delta n_{3_+} \frac{\mathrm{d}\ln C_{3^+}}{\mathrm{d}\ln C} + \Delta n_{2^+} \frac{\mathrm{d}\ln C_{2^+}}{\mathrm{d}\ln C} \qquad \mathbf{5}$$

The apparent Δn is now the weighted sum from each ion form produced by addition of the trichloride salt. This behavior, shown as the solid line in Figure 3, gives a reasonable description of the data across the entire range of multivalent cation concentrations with no fitting parameters. The negative slope of the force versus concentration curve indicates replacement of bound 2^+-ions with 3^+-ions as DNA condenses; ion pairing accounts for the resolubilization observed in the magnetic tweezers data. This peculiar behavior appears to be more likely a consequence of multivalent cation chemistry than new polyelectrolyte physics.

If this ion-binding model is correct, then it should also be able to describe variations in the phase diagram as monovalent salt concentration, C_{1^+}, is changed. Experimental measurements of the spermidine/monovalent cation phase diagram performed by Raspaud *et al.* (9) are reproduced in Figure 7. At the boundaries of the phase diagram, the Gibbs–Duhem gives a constraint on the slope of the boundary (Appendix C),

$$\frac{\mathrm{d}\ln C}{\mathrm{d}\ln C_1} = -\frac{\sum_{i=1^+,2^+,3^+} \Delta n_i (\mathrm{d}\ln C_i/\mathrm{d}\ln C_1)}{\sum_{i=2^+,3^+} \Delta n_i (\mathrm{d}\ln C_i/\mathrm{d}\ln C)} \qquad \mathbf{6}$$

We use our measured critical point, $C = 1.8 \times 10^{-4}$ M at $C_1 = 8 \times 10^{-3}$ M and then integrate Equation (6) to obtain the solid line on Figure 3. Concentrations and Δn_i were calculated identically to Equation (5). The agreement is quite good, again, with no fitting parameters.

It is remarkable that nowhere in our analysis have we considered alterations in the DNA–DNA attractive interactions, taking into account only the changes in free energy associated with binding neutralizing cations. Yet, variations in the free energy with spermidine concentration, and also, the location of phase boundaries are well described without any free parameters. This suggests that, although interhelical interactions between condensed DNA show some dependence on electrolyte concentration (8,24), the energetic consequences of this variation are small compared to the energetic cost of binding neutralizing multivalent cations. Since ion-binding energies dominate the electrolyte dependence of DNA condensation, it would be difficult to use the electrolyte dependence of DNA condensation to elucidate the mechanism of DNA–DNA attraction. Any, relatively small, contribution from the electrolyte dependence of DNA–DNA attractions could be incorporated as a correction to our model to improve the agreement with experimental data.

CONCLUSION

In contrast to the traditional assumption that DNA condensation produces a change in number of bound counterions that is *larger* for $Co(NH_3)_6^{3+}$ than for spermidine^{3+} (28,29), our measurements show that the change in bound counterions is actually *smaller* for $Co(NH_3)_6^{3+}$ than for spermidine. This decrease in the number of ions required to bind upon condensation allows $Co(NH_3)_6^{3+}$ to affect condensation at a lower critical concentration. The traditional Manning–Oosawa counterion adsorption model could describe variations in the condensation force near the critical points in the dilute regime. Variations in condensation force over the entire range of concentrations and the spermidine^{3+}/Na^{+} phase diagram of Raspaud *et al.* (9) could be described by the same model, if the counterion–anion pairing that occurs at high concentrations was included. In short, provided that counterion chemistry is treated properly, the traditional Manning–Oosawa adsorption isotherm appears capable of predicting the counterion concentration dependence for DNA condensation without invoking overcharging or any changes in the condensed state via, for instance, electrolyte screening.

ACKNOWLEDGMENTS

This research was supported by the Intramural Program of the National Institute of Child Health and Human Development at the National Institutes of Health. BAT and DCR thank Dr V. Adrian Parsegian and Dr Sergey Leiken for helpful discussions. BAT thanks Prof. Sanford Leuba for advice on magnetic tweezing of DNA and also gratefully acknowledges support from the labs of Dr Paul D. Smith and Thomas J. Pohida. Funding to pay the Open Access publication charges for this article was provided by the Intramural Program of the National Institute for Child Health and Human Development.

Conflict of interest statement. None declared.

REFERENCES

1. Bloomfield,V.A., Crothers,D.M. and Tinoco,I. (2000) *Nucleic Acids Structure, Properties, and Functions* University Science Books, Sausalito.
2. Keyser,U.F., Koeleman,B.N., van Dorp,S., Krapf,D., Smeets,R.M.M., Lemay,S.G., Dekker,N.H. and Dekker,C. (2006) Direct force measurement on DNA in a solid-state nanopore. *Nature Physics*, **2**, 473–477.
3. de Frutos,M., Brasiles,S., Tavares,P. and Raspaud,E. (2005) Effect of spermine and DNase on DNA release from bacteriophage T5. *Eur. Phys. J. E*, **17**, 429–434.
4. Arya,G. and Schlick,T. (2006) Role of histone tails in chromatin folding revealed by a mesoscopic oligonucleosome model. *Proc. Nat. Acad. Sci. USA*, **103**, 16236–16241.
5. Range,K., Mayaan,E., Maher,L.J. and York,D.M. (2005) The contribution of phosphate-phosphate repulsions to the free energy of DNA bending. *Nucleic Acids Res.*, **33**, 1257–1268.
6. Manning,G.S. (1978) Molecular theory of polyelectrolyte solutions with applications to electrostatic properties of polynucleotides. *Q. Rev. Biophys.*, **11**, 179–246.
7. Wilson,R.W., Rau,D.C. and Bloomfield,V.A. (1980) Comparison of poly-electrolyte theories of the binding of cations to DNA. *Biophys. J.*, **30**, 317–325.
8. Yang,J. and Rau,D.C. (2005) Incomplete ion dissociation underlies the weakened attraction between DNA helices at high spermidine concentrations. *Biophys. J.*, **89**, 1932–1940.
9. Raspaud,E., Olvera de la Cruz,M., Sikorav,J.-L. and Livolant,F. (1998) Precipitation of DNA by polyamines: A polyelectrolyte behavior. *Biophys. J.*, **74**, 381–393.
10. Raspaud,E., Chaperon,I., Leforestier,A. and Livolant,F. (1999) Spermine-induced aggregation of DNA, nucleosome, and chromatin. *Biophys. J.*, **77**, 1547–1555.
11. Pelta,J., Livolant,F. and Sikorav,J.-L. (1996) DNA aggregation induced by polyamines and cobalthexamine. *J. Biol. Chem.*, **271**, 5656–5662.
12. Pelta,J., Durand,D., Doucet,J. and Livolant,F. (1996) DNA mesophases induced by spermidine: Stuctural properties and biological implications. *Biophys. J.*, **71**, 48–63.
13. Olvera de la Cruz,M., Belloni,L., Delsanti,M., Dalbiez,J.P., Spalla,O. and Drifford,M. (1995) Precipitation of highly charged polyelectrolyte solution in the presence of multivalent salts. *J. Chem. Phys.*, **103**, 5781–5791.
14. Golestanian,R. and Liverpool,T.B. (2002) Conformational instability of rodlike polyelectrolytes due to counterion fluctuations. *Phys. Rev. E. Stat. Nonlin. Soft Matter Phys.*, **66**, 051802.
15. Zhang,R. and Shklovskii,B.I. (2005) The pulling force of a single DNA molecule condensed by spermidine. *Physica A*, **349**, 563–570.
16. Nguyen,T.T., Rouzina,I. and Shklovskii,B.I. (2000) Reentrant condensation of DNA induced by multivalent counterions. *J. Chem. Phys.*, **112**, 2562–2568.
17. Grosberg,A.Y., Nguyen,T.T. and Shklovskii,B.I. (2002) Colloquium: the physics of charge inversion in chemical and biological systems. *Rev. Mod. Phys.*, **74**, 329–345.
18. Besteman,K., Van Eijk,K. and Lemay,S. (2007) Charge inversion accompanies DNA condensation by multivalent cations. *Nature Physics*, doi:10.1038/nphys1697.
19. Solis,F.J. and Olvera de la Cruz,M. (2001) Flexible linear polyelectrolytes in multivalent salt solutions: Solubility conditions. *Eur. Phys. J. E.*, **4**, 143–152.
20. Solis,F.J. (2002) Phase diagram of dilute polyelectrolytes: Collapse and redissolution by association of counterions and co-ions. *J. Chem. Phys.*, **117**, 9009–9015.
21. Conwell,C.C., Vilfan,I.D. and Hud,N.V. (2003) Controlling the size of nanoscale toroidal DNA condensates with static curvature and ionic strength. *Proc. Nat Acad. Sci. USA*, **100**, 9296–9301.
22. Hud,N.V. and Downing,K.H. (2001) Cryoelectron microscopy of lambda phage DNA condensates in vitreous ice: The fine structure of DNA toroids. *Proc. Natl Acad. Sci. USA*, **98**, 14925–14930.
23. Hud,N.V. and Vilfan,I.D. (2005) Toroidal DNA condensates: unraveling the fine structure and the role of nucleation in determining size in vitro. *Ann. Rev. Biophys. Biomol. Struc*, **34**, 295–318.
24. Raspaud,E., Durand,D. and Livolant,F. (2005) Interhelical spacing in liquid crystalline spermine and spermidine-DNA precipitates. *Biophys. J.*, **88**, 392–403.
25. Rau,D.C. and Parsegian,V.A. (1992) Direct measurement of the intermolecular forces between counterion-condensed DNA double helices: Evidence for long range attractive hydration forces. *Biophys. J.*, **61**, 246–259.
26. Plum,G.E. and Bloomfield,V.A. (1988) Equilibrium dialysis study of binding of hexammine cobalt(III) to DNA. *Biopolymers*, **27**, 1045–1051.
27. Braunlin,W.H., Strick,T.J. and Record,M.T. (1982) Equilibrium dialysis studies of polyamine binding to DNA. *Biopolymers*, **21**, 1301–1314.
28. Wilson,R.W. and Bloomfield,V.A. (1979) Counterion-induced condensation of Deoxyribonucleic Acid. A light-scattering study. *Biochem.*, **18**, 3192–2196.
29. Matulis,D., Rouzina,I. and Bloomfield,V.A. (2000) Thermodynamics of DNA binding and condensation: Isothermal titration calorimetry and electrostatic mechanism. *J. Mol. Biol.*, **296**, 1053–1063.
30. Todd,B.A, Parsegian,V.A., Shirahata,A., Thomas,T.J. and Rau,D.C. (in preparation) Attractive forces between cation condensed DNA helices.
31. Baumann,C.G., Smith,S.B., Bloomfield,V.A. and Bustamante,C. (1997) Ionic effects on the elasticity of single DNA molecules. *Proc. Natl Acad. Sci. USA*, **94**, 6185–6190.
32. Baumann,C.G., Bloomfield,V.A., Smith,S.B., Bustamante,C., Wang,M.D. and Block,S.M. (2000) Stretching of single collapsed DNA molecules. *Biophys. J.*, **78**, 1965–1978.
33. Murayama,Y., Sakamaki,Y. and Sano,M. (2003) Elastic response of single DNA molecules exhibits a reentrant collapsing transition. *Phys. Rev. Lett.*, **90**, 018102.
34. Besteman,K., Hage,S., Dekker,N. and Lemay,S. (2007) Role of tension and twist in single-molecule DNA condensation. *Phys. Rev. Lett.*, **98**, 058103.
35. Rouzina,I. and Bloomfield,V.A. (1996) Macroion attraction due to electrostatic correlation between screening counterions. 1. Mobile surface-absorbed ions and diffuse ion cloud. *J. Phys. Chem.*, **100**, 9977–9989.
36. Braunlin,W.H. and Xu,Q.W. (1992) Hexaamminecobalt (III) binding environments on double-helical DNA. *Biopolymers*, **32**, 1703–1711.
37. Xu,Q.W. and Braunlin,W.H. (1992) Sequence specific cobalt(III) cation binding-sites on DNA. *FASEB J.*, **6**, A362–A362.
38. Braunlin,W.H., Anderson,C.F. and Record,M.T. (1987) , Competitive interactions of $Co(NH_3)_6^{3+}$ and Na^+ with helical B-DNA probed by Co-59 and Na-23 NMR. *Biochemistry*, **26**, 7724–7731.
39. Tang,J.X., Janmey,P.A., Lyubartsev,A. and Nordenskiold,L. (2002) Metal ion-induced lateral aggregation of filamentous viruses fd and M13. *Biophys. J.*, **83**, 566–581.
40. Jenkins,I.L. and Monk,C.B. (1951) The conductivities of some complex cobalt chlorides and sulfates. *J. Chem. Soc.*, **68**, 73.
41. Evans,M.G. and Nancollas,G.H. (1953) Spectrophotometric investigations of some complex cobaltic chloro, bromo, iodo, and azide ion-pairs. *Trans. Faraday Soc.*, **49**, 363–371.
42. Record,M.T. (1975) Effects of Na+ And Mg++ ions on helix-coil transition of DNA. *Biopolymers*, **14**, 2137–2158.
43. Manning,G.S. (1972) Application of polyelectrolyte limiting laws to helix-coil transition of DNA.1. Excess univalent cations. *Biopolymers*, **11**, 937.

APPENDIX A

We begin with the Gibbs–Duhem equation at constant temperature and pressure,

$$\sum_i N_i \mathrm{d}\mu_i = 0. \qquad \textbf{A1}$$

This equation provides a constraint on changes in component chemical potential, μ_i weighted by the number of that component N_i. For a single, stretched

DNA chain $N_{DNA} = 1$. The DNA chemical potential can be written as a sum of the chemical potential of the entire DNA chain, μ_{DNA} plus a potential energy due the unidirectional force field, f imposed along the direction of extension, X,

$$d\mu_{DNA} - Xdf + \sum_{i \neq DNA} N_i d\mu_i = 0. \quad \textbf{A2}$$

In solution, there are two DNA phases in equilibrium, extended and condensed. We consider how the DNA chemical potential difference—synonymous with the DNA free energy difference—between the two phases varies as a function of the other components in solution and with the applied force,

$$d\Delta\mu_{DNA} - \Delta X df + \sum_i \Delta N_i d\mu_i = 0, \quad \textbf{A3}$$

where ΔX is the difference in the extension of the DNA across the transition and ΔN_i is the difference in the number of molecules of the i-th component associated the DNA between with the two states.

At the transition force between extended and condensed forms, $f = f_c$, the DNA chemical potential difference is at a minima, i.e. $d\Delta\mu_{DNA} = 0$. This yields an equation,

$$\Delta X df_c = \sum_i \Delta N_i d\mu_i \quad \textbf{A4}$$

that equates the 'extrinsic' mechanical and chemical work done across the condensing transition. It can be related to the 'intrinsic' physical parameters for DNA by dividing through by the contour length of the DNA,

$$l\Delta x df_c = \sum_i \Delta n_i \, d\mu_i, \quad \textbf{A5}$$

where $\Delta x = \Delta X/L$, $\Delta n_i = \Delta N_i/N_p$, is the change in ions bound per phosphate, N_p is the total number of phosphates, and $l = 1.7$ Å is the average contour length between DNA phosphates. For forces >1 pN the DNA end-to-end extension, X is nearly equal to the contour length, L, so, $\Delta x \approx 1$. At smaller forces, Δx can be obtained from the measured DNA end-to-end extension at the onset of collapse, divided by the known DNA contour length. Equation (A5) forms the basis for all subsequent calculations. We neglect nonideality in the component chemical potentials throughout, so that, they are simply related to the component concentrations, C_i, by $\mu_i = k_b T \ln C_i$.

Changing C near the critical point

At low concentrations of the trichloride salt added to solution, C, both spermine trichloride and $Co(NH_3)_6Cl_3$ completely dissociate to give an equal concentration of the trivalent ion, C_{3+}. Neglecting the contribution of the anion, and holding the concentration of $Tris^+$ constant, this changes the chemical potential of one component. This reduces the sum in Equation (A5) to a single term

$$l\Delta x df_c = \Delta n_{3+} d\mu_{3+}. \quad \textbf{A6}$$

Substituting $\mu_{3+} = k_b T \ln C$ and rearranging gives,

$$\frac{l\Delta x}{k_b T} \frac{df_c}{d\ln C} = \Delta n_{3+} \quad \textbf{A7}$$

Hence, at dilute concentrations, the change in bound trivalent cations upon condensation can be evaluated directly from the experimentally measured slope of f_c versus $\ln C$.

In addition, we have compared the measured Δn_{3+} with a model. Consistent with our measured 0.33 $Co(NH_3)_6^{3+}$/phosphate ratio in the DNA condensate (Figure 4), we assume that the +3 ion completely and exclusively neutralizes the condensed DNA. The number of ions bound to the extended DNA is calculated based on Manning–Oosawa theory (6), neglecting a ~10% additional contribution from screening of the residual DNA charge (1,42,43). Manning–Oosawa theory accurately predicts the electrolyte sensitivity of DNA–cation binding, though not its absolute magnitude (26). It is largely equivalent to other mean-field electrostatic theories such as, the Poisson–Boltzmann equation (7). For a displacement of bound ions by +3 ions in the extended to condensed transition, we have,

$$\begin{aligned} i = 3^+ \quad & \Delta n_i = 1/3 - \theta_i \\ i \neq 3^+ \quad & \Delta n_i = -\theta_i \end{aligned} \quad \textbf{A8}$$

where θ_i is the fraction of the i–th ion bound to DNA in the extended state, respectively, calculated within the Manning–Oosawa formulism (relevant equations recapitulated in Appendix D) (6). They are evaluated in terms of the concentrations of each species, the standard linear charge density of DNA, $1e^-$ per 1.7 Å, and the Bjerrum length in liquid water at 298 K, 7.16 Å. There are no free parameters. The model (dashed line in Figure 3) is close to overlapping the data at lower concentrations.

Appendix B: Changing C over entire range

At intermediate and high concentrations, dissociation of the trichloride salt is incomplete; a total concentration, C of the trichloride salt produces a certain concentration of trivalent cations, C_{3+} and a certain concentration of anion-paired divalent ions, C_{2+}. Since this changes the chemical potentials of two components, we require two terms from the sum of Equation (A5),

$$l\Delta x df_c = \Delta n_{3+} d\mu_{3+} + \Delta n_{2+} d\mu_{2+}. \quad \textbf{B1}$$

The chemical potentials for the two components are not however, independent. They are constrained by the material balances,

$$\begin{aligned} C &= C_{3+} + C_{2+} \\ C_{1-} &= 3C_{3+} + 2C_{2+} \end{aligned} \quad \textbf{B2}$$

and the equilibrium between 3^+ and 2^+ cations,

$$3^+ + 1^- \underset{K_{ion-pair}}{\longleftrightarrow} 2^+; \quad K_{ion-pair} = \frac{C_{3+}C_{1-}}{C_{2+}}. \quad \textbf{B3}$$

These three equations constrain the four concentrations so that, C, the concentration of the trichloride salt added

to solution is the only degree of freedom. This allows us to write the chemical potentials for each component in terms of the experimental control variable,

$$d\mu_i = k_b T \frac{d \ln C_i}{d \ln C} d \ln C. \quad \textbf{B4}$$

Inserting into Equation (B1) we have,

$$\frac{l \Delta x}{k_b T} \frac{df_c}{d \ln C} = \Delta n_{3+} \frac{d \ln C_{3+}}{d \ln C} + \Delta n_{2+} \frac{d \ln C_{2+}}{d \ln C} \quad \textbf{B5}$$

The sensitivity of condensation force to the concentration of trivalent cation salt added to solution now consists of the weighted contribution of the 3^+ and 2^+ forms of the ion. The $d\ln C_i/d\ln C$ terms can be directly evaluated from the material balances and equilibrium between 3^+ and 2^+. The change in number of bound ions of each species is calculated as before based on Manning–Oosawa theory. Taking the equilibrium constant relating concentrations of 3^+ and 2^+ ions from a previous estimate for spermidine, $K_{\text{ion-pair}} = 0.15\,\text{M}$ (8) gives the solid line in Figure 3. Again, there are no free parameters.

Appendix C. Phase boundaries for trivalent and monovalent concentrations

Raspaud *et al.* measured the phase boundaries for DNA condensation as a function of spermidine trichloride and NaCl concentration added to solution, C_1 (9). This situation is also governed by the Gibbs–Duhem equation (Equation A5) but with no external force,

$$0 = \Delta n_{3+} d\mu_{3+} + \Delta n_{2+} d\mu_{2+} + \Delta n_{1+} d\mu_{1+}. \quad \textbf{C1}$$

As before, the chemical potentials are not independent. Introducing the equilibrium between 3^+ and 2^+ ions and the material balances reveals the two independent degrees of freedom C and C_1. Each chemical potential can be written as a weighted contribution of these two degrees of freedom,

$$d\mu_i = k_b T \frac{d \ln C_i}{d \ln C} d \ln C + k_b T \frac{d \ln C_i}{d \ln C_1} d \ln C_1 \quad \textbf{C2}$$

Inserting this into Equation (C1) and rearranging gives the slope of the phase diagram,

$$\frac{d \ln C}{d \ln C_1} = - \frac{\sum_{i=1+,2+,3+} \Delta n_i (d \ln C_i / d \ln C_1)}{\sum_{i=2^+,3^+} \Delta n_i (d \ln C_i / d \ln C)} \quad \textbf{C3}$$

This equation is integrated from the experimentally measured critical points for spermidine, $C = 1.5 \times 10^{-4}\,\text{M}$ and $C_1 = 0.008\,\text{M}$, and using the same parameters given in Appendix B to obtain the line in Figure 3. Again there are no free parameters.

Appendix D. Manning–Oosawa Formalism

The Manning–Oosawa formalism is used to calculate the fractional binding θ_i (per unit of polyelectrolyte charge) of a Z_i-valent counterion i, around a line charge with linear charge density b in a medium of Bjerrum length l_b. The ratio of the linear charge density to the Bjerrum length, $\xi = b/l_b$ is sometimes called the 'Manning parameter'. Manning–Oosawa condensation is reviewed extensively in ref. (6) so, we only briefly describe it here, giving equation numbers from that reference for further details. Each θ_i, is calculated by minimizing a free energy composed of the electrostatic interaction between the ion and the line charge, the mixing free energy of the bound ions, the mixing free energy of the unbound ions, and an osmotic term for the unbound ion. The expression for the free energy is straightforward so, the minimum can be found from the zero of an analytical expression for the derivative of the free energy with respect to θ_i. Each θ_i satisfies an equation of the form [similar to Equation (53)–(54) in ref. (6), generalized for an arbitrary number of ions],

$$0 = 2 Z_i \xi \left(1 - \sum_i Z_i \theta_i\right) \times \ln\left(1 - e^{-\kappa b}\right) + \ln(\theta_i / V_i) - \ln(C_i/1000) + 1 \quad \textbf{D1}$$

where, C_i, and V_i are the bulk concentration (M) and volume of the bound territory (cm^3) for the i-th counterion, respectively. The inverse screening length κ is

$$\kappa = 0.0869 \sqrt{l_b \sum_i C_i Z_i^2} \quad \textbf{D2}$$

where l_b and $1/\kappa$ are in units Å. Assuming that all of the coions (Cl^- in our case) are monovalent, the volume of the bound territories are given by Equation (13) in Ref. (6),

$$V_i = 4\pi e L_{AV} (1 + Z_i)(\xi - 1/Z_i) b^3 \quad \textbf{D3}$$

where L_{AV} is Avogadro's number. We verified our numerical solutions by reproducing Table 5 in ref. (6) for the case, $\xi = 4.6$ and $V_1 = V_2 = 646\,\text{cm}^3$.